UCC

University College Cork, Ireland
Coláiste na hOllscoile Corcaigh

III-V electro-absorption modulation and detection devices integrated to 220 nm silicon-on-insulator

Owen Moynihan [0009-0002-3345-7085], Samir Ghosh, James O'Callaghan, Brendan Roycroft, Kevin Thomas, Emanuele Pelucchi, and Brian Corbett

Tyndall National Institute, University College Cork, Ireland
*owen.moynihan@tyndall.ie

Abstract III-V indium phosphide (InP) ridge coupons capable of electro-absorption modulation and detection are integrated on a 220 nm silicon-on-insulator platform using transfer printing. The coupons employ a PIN structure design that can be actively biased to efficiently modulate and detect light with a bandwidth of >30 nm from 1550 nm – 1580 nm. Across the C-band, the grating coupled devices provide an extinction ratio (ER) of 25 dB and detect light with a responsivity of over 0.85 A/W, with an insertion loss (IL) at 0 V of 3.5 dB at 1580 nm and 6.5 dB at 1550 nm.

Keywords: Heterogeneous integration, micro-transfer printing, electro-optic modulation, photo-detection, Quantum-confined-Stark-effect (QCSE)

1 Introduction

While silicon photonics (SiPh) comprising of silicon-on-insulator (SOI), is the predominant photonics integrated circuit (PIC) platform [1], there are still drawbacks when considering its limited active device selection. For example, SiPh does not have an efficient monolithic laser/amplifier due to its indirect bandgap [2], while modulation is limited to carrier dispersion effects. This results in several millimetres of device length for Mach-Zehnder interferometers or high fabrication precision and low spectral bandwidth for micro-ring resonator modulator configurations [3]. Due to these limitations, the silicon modulator performance remains inferior to InP-based modulators. Germanium (Ge) detectors involve multiple additional fabrication steps such as dopant implants and high-temperature processes. One solution to these issues is the heterogeneous integration of active devices composed of suitable materials such as III-V and lithium niobate onto SiPh. This integration can take place via flip-chip mounting [4], wafer bonding [5] or micro-transfer printing (µTP) [6].

In this work, III-V PIN waveguide coupons are fabricated and integrated on 220 nm SOI via transfer printing. The waveguiding, modulation and detection characteristics are measured through both surface normal absorption and waveguide transmission using external vertical grating coupling. The InAlGaAs multiple quantum well (MQW) structures act as both electro-absorption modulator (EAM) and photodiode (PD). While most PDs work far above the bandgap of the absorber material, this device intentionally works through the band edge, utilizing the quantum confined Stark effect (QCSE) to spectrally modulate and detect light by application of voltage [7]. A ridge waveguide design is implemented for a long absorption length, or transparent guiding, as needed. This is the first time a transfer printed III-V EAM device has been designed and produced for SiPh, to the best of the authors knowledge.

2 Device Design and Fabrication

The epitaxial structure was grown on an InP substrate, consisting of a thin (200 nm) n-InP region, an intrinsic region including a 10 layer MQW active region and a thick (1600 nm) p-InP region, with an InGaAs p-contact layer. The QCSE shift was measured using a 1 mm diameter mesa PIN diode test structure with annular contacts via surface normal absorption, which can be seen in Fig. 1(a). With biasing from 0 V to -10 V, a band-edge shift is of >100 nm is measured (1528 nm to 1648 nm). Fig. 1(b) shows the quadratic dependence of the absorption band edge energy with the applied voltage.

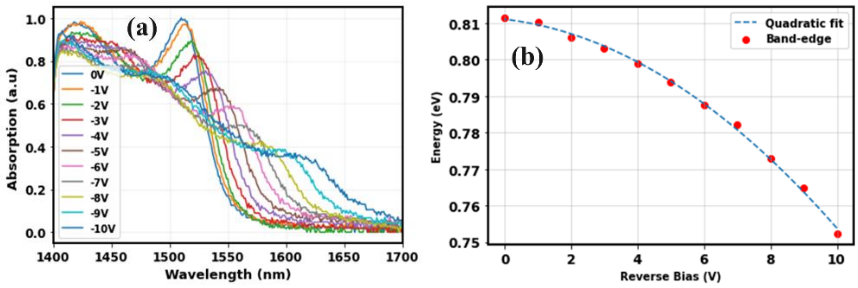

Fig. 1. (a) Surface normal absorption spectrum from 0 V to -10 V of the III-V epitaxial structure and (b) the extracted band-edge energy as a function of voltage.

An evanescently coupled ridge was designed for the III-V - SOI integration (Fig. 2(a)), whereby the coupon is printed directly on the SOI waveguide. The III-V ridge was designed to have a high mode overlap with the active region, with the simulated QW overlap being 22.5 %, for a 3 µm wide ridge. Using the collinear silicon waveguide, the overlap with the loss-inducing p-doped region is 12.0 % compared to 14.2 % without the underlying silicon. The coupling to/from the ridge was designed using tapers to gradually move the light between the SOI waveguide and III-V ridge. Through simulations, the taper was designed to maintain a single-mode transition from the SOI to the EAM for high transmission between the waveguides, with 99 % transmission for zero and 62 % for 0.5 µm misalignment, respectively. The coupons, comprising of partially finished devices, were fabricated using combined electron-beam and optical lithography together with plasma etching to define the ridge, n-metal, coupon, and photoresist tethers, which were then undercut using a diluted $FeCl_3$ solution. SOI waveguides and gratings were fabricated using electron-beam lithography and plasma etching. The devices were printed directly to the 220 nm SOI over the waveguide structure, where the bond pads were then deposited. The printing accuracy was measured to be ±0.5 µm. The device design cross-section when printed to the SOI substrate and fabricated device with lithography layers are shown in Fig. 2.

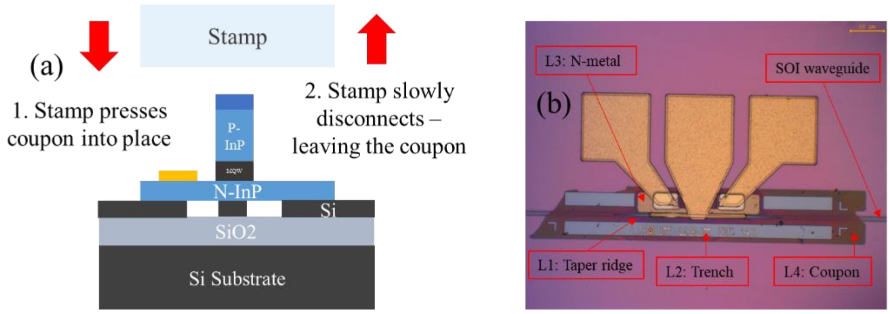

Fig. 2. (a) A schematic of the device cross-section (not to scale) and integration technique. (b) Integrated device and its components.

3 Device Characteristics

A 3 µm ridge with a device length (including in/out tapers of 100 µm) of 250 µm was measured by coupling light in and out of the circuit and measuring the transmission power and modulator photocurrent as a function of wavelength and bias. The waveguide power was extracted by transmission measurements of a reference circuit without a modulator. Fig. 3 (a) shows the measured photocurrent vs. wavelength at different biases. The extracted transmission spectra of the device at different biases are shown in in Fig. 3 (b), which were used to calculate the extinction ratio (ER) and insertion loss (IL). Fabry-Perot fringes are measured in the spectra, which are due to the SOI waveguide taper between the grating and the single-mode waveguide region. For the best device (assumed zero misalignment), a 30 dB ER for a bias between 0 V to -6 V together with an IL of 6.5 dB was measured at 1550 nm. The ER remains greater than 25 dB across 1565 nm to 1580 nm with biasing from 0 V to -8 V, with an IL of 3.5 dB. The higher IL at 1550 nm is due to residual band edge absorption. The static characterization has a performance equivalent to state-of-the-art EAM modulation in monolithic InP platforms, in terms of ER and IL [8].

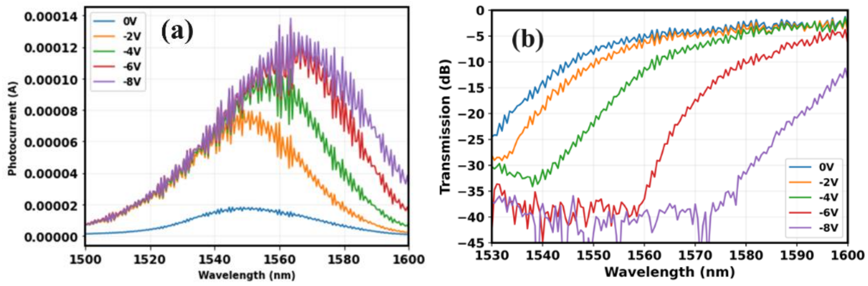

Fig. 3. (a) Received photocurrent vs. wavelength as a function of reverse bias after transmission through the circuit, including grating couplers, (b) extracted transmission vs wavelength for the modulator from 0 V to -8 V, confirming QCSE shift in the integrated device.

The detection characteristics similarly utilize the QCSE effect to shift the normally transparent material to absorb. The responsivity from 1550 nm to 1580 nm vs bias is shown in Fig. 4(a) and a comparison of the light vs dark current is shown in Fig. 4(b). As the material is mostly transparent without bias, there is very low responsivity at 0 V for 1550 nm. With increased bias, efficient absorption of light is achieved (at bias > -4 V) where a responsivity of 0.85 A/W and higher is calculated. This responsivity is calculated by measuring the light power before entering the circuit and subtracting the loss from the grating coupler (assuming two grating couplers are identical) of a reference grating (loss = 5.2 dB). As the taper is actively absorbing, the simulated loss from the taper misalignment is not included (~0.8 dB), and this is a lower bound for responsivity. The detection quantum efficiency is calculated to be 87 % for wavelengths 1570 nm and 1580 nm at -8 V.

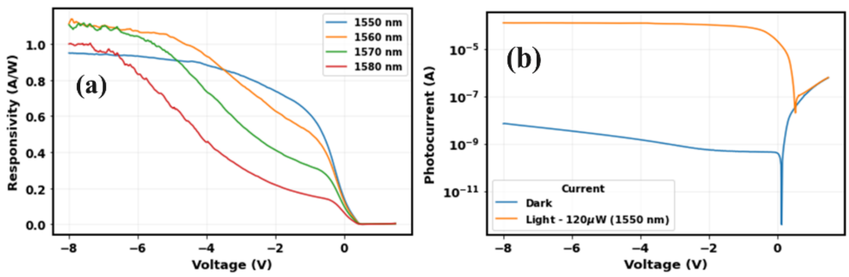

Fig. 4. (a) Responsivity vs. bias for 1550 nm to 1580 nm, (b) Comparison of light and dark current at 1550 nm.

4 Conclusion

InP EAM/PD device coupons have been successfully integrated on to a 220 nm SOI platform using transfer printing with their transmission and absorption characteristics measured. The devices are capable of functioning as a modulator and detector, displaying a responsivity of over 0.85 A/W at -4 V and an ER of > 30 dB at 1550 nm, with an overall 25 dB ER over a 30 nm range. The IL is measured to be 6.5 dB and 3.5 dB for 1550 nm and 1580 nm respectively. The QCSE shift in the material was over 100 nm at -10 V and can be used to spectrally modulate transmission and absorption.

5 Acknowledgements

This work was supported by SFI through IPIC (12/RC/2276-P2) and the PIADs programme. The authors acknowledge the fabrication facility and services at Tyndall National Institute.

REFERENCES

1. W. Bogaerts and L. Chrostowski, "Silicon Photonics Circuit Design: Methods, Tools and Challenges," *Laser and Photonics Reviews*. 2018. doi: 10.1002/lpor.201700237.
2. P. Kaur, A. Boes, G. Ren, T. G. Nguyen, G. Roelkens, and A. Mitchell, "Hybrid and heterogeneous photonic integration," *APL Photonics*, vol. 6, no. 6. 2021. doi: 10.1063/5.0052700.
3. G. T. Reed, G. Mashanovich, F. Y. Gardes, and D. J. Thomson, "Silicon optical modulators," *Nature Photonics*. 2010. doi: 10.1038/nphoton.2010.179.
4. A. Marinins *et al.*, "Wafer-Scale Hybrid Integration of InP DFB Lasers on Si Photonics by Flip-Chip Bonding With sub-300 nm Alignment Precision," *IEEE J. Sel. Top. Quantum Electron.*, 2023, doi: 10.1109/JSTQE.2022.3223641.
5. Y. Tang, J. D. Peters, and J. E. Bowers, "Over 67 GHz bandwidth hybrid silicon electroabsorption modulator with asymmetric segmented electrode for 13 μm transmission," *Opt. Express*, 2012, doi: 10.1364/oe.20.011529.
6. B. Corbett, R. Loi, J. O'Callaghan, and G. Roelkens, "Transfer Printing for Silicon Photonics," in *Semiconductors and Semimetals*, vol. 99, 2018. doi: 10.1016/bs.semsem.2018.08.001.
7. D. A. B. Miller *et al.*, "Band-edge electroabsorption in quantum well structures: The quantum-confined stark effect," *Phys. Rev. Lett.*, vol. 53, no. 22, 1984, doi: 10.1103/PhysRevLett.53.2173.
8. M. Trajkovic, F. Blache, H. Debregeas, K. A. Williams, and X. J. M. Leijtens, "Increasing the Speed of an InP-Based Integration Platform by Introducing High Speed Electroabsorption Modulators," *IEEE J. Sel. Top. Quantum Electron.*, 2019, doi: 10.1109/JSTQE.2019.2913727.